

Optimal Flower Pollination Based Nonlinear PID Controller for Pantograph Robot Mechanism

Layla M EL-Tehewy

Mechatronics Engineering Department, MTI University, Cairo, Egypt

Email: Laylaa.mahmoud@eng.mti.edu.eg

Mohamed A. Shamseldin¹, Mohamed Sallam², and A. M. Abdel Ghany³

¹ Mechanical Engineering Department, Future University in Egypt, Cairo, Egypt

² Mechanical Engineering Department, Helwan University, Cairo, Egypt

³ Higher Engineering Institute, Thebes Academy, (on Leave From Helwan University), Cairo, Egypt

Email: Mohamed.abelbbar@fue.edu.eg, sallam.mohamed@h-eng.helwan.edu.eg, and

Abdelghany.mohamed@thebes.edu.eg

Abstract—Pantograph Robot Mechanism is considered a type of parallel manipulator which has been developed largely for industrial applications that need high accuracy and speed. Whereas, it needs a high-performance controller to track preselected trajectory planning. It is also able to carry higher weights than the open-chain mechanism with suitable accuracy and stability; this is because it consists of four active links and one passive link, instead of two links as in the open chain. This study presents a mathematical model for a closed chain pantograph mechanism, where the boundary conditions are taken into account. A complete MATLAB Simulink has been developed to simulate the dynamics of the pantograph robot mechanism. To validate the proposed mathematical model of the pantograph, the corresponding Simscape model had been developed. Also, two different tracking controllers were designed. The first control is the PID controller which had optimized by Flower Pollination (FP) optimization. The second control is an enhanced Nonlinear PID (NLPID) controller where its parameters were obtained by Flower Pollination (FP) optimization based on the effective objective function. A rectangular trajectory was selected to be a position reference of the end effector of the pantograph robot. This task was done using the proposed controllers to investigate the performance. The results show that the NLPID controller-based FP has a better performance compared to the PID controller. The end effector has a less rise time and settling time with high accuracy in the case of the NLPID controller.

Index Terms—flower pollination, pantograph robot, Nonlinear PID (PID), manipulator dynamics

I. INTRODUCTION

Parallel robots have become a necessary part of the robots used in academia and industry [1]. Besides, with the rapid development of parallel robots, the research on mechanism theory, mobility analysis, dimensional synthesis, kinematics and dynamics modeling, and design optimization has been increasing on a large scale [2]. The development of parallel robotics and controllable

mechanism has become widely used as a mechanical design, as shown in Fig. 1 [3].

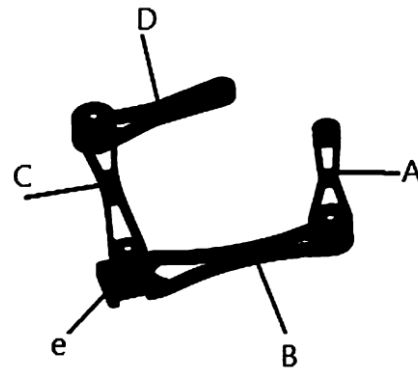


Figure 1. Five bar planar (Pantograph).

The name pantograph refers to the five-sided links used. Four of the five links are moving platforms and the fifth one is the base platform [4]. The five-bar planar manipulator is a relatively simple mechanism that has two-degree-of-freedom (DOF) and its kinematics is explicit [5]. However, its characteristics are high speed, high accuracy, low inertia, and carrying more weights [6].

For these reasons, it draws a lot of researchers' attention. Some prototypes and commercial products were made, such as the 'double SCARA' RP-AH series offered by Mitsubishi Electric, and DexTAR, a five-bar planar manipulator designed by ETS. The five-links planar of the pantograph, which is a simple two degree of freedom (DOF) mechanism (Fig. 2), one of them (L0) is passive and the other four links (L1, L2, L3, L4) are active.

The system contains only five revolute joints (Fig. 2). Links 1 and 4 are the driving links. With the help of the appropriate rotation of the actuating links, the characteristic point e of the system can follow the desired planar trajectory in the region of the working zone [7]. Especially, the need for exactly adaptive automation in

varied applications has led to higher requirements for operational accuracy and cycle time with robots [8]. Examples of such needs are higher precision assembly, faster product handling, surface finishing, better measurements, surface finishing, and milling capabilities [9]. Additionally, there is a high demand for off-line programming to eliminate touch-up of programmed positions; in other words, robots must perform their task with better load capacity and accuracy in operations. A general trend of meeting these requirements is to make use of parallel robots, which have excellent potential capabilities, including high rigidity, high accuracy, and high loading capacities [10].

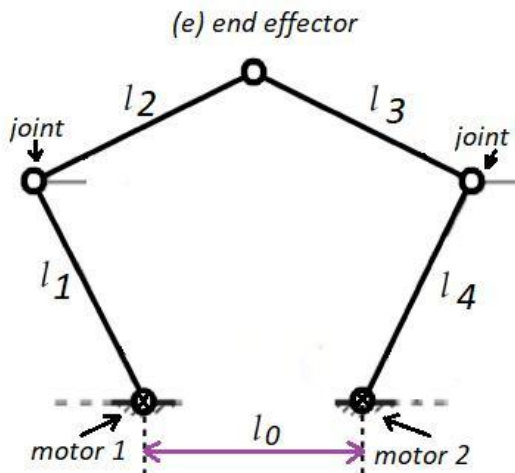


Figure 2. Two-DOF mechanism.

The PID controller is linear and commonly used in engineering applications because of its simple scheme and satisfying performance. Its gains are adjusted to assure both stability and performance. For such purpose, several design techniques were suggested in particular, intelligent techniques (Genetic Algorithm (GA), Evolutionary Programming (EP), and Simulated Annealing (SA), etc..) and animal mimics (Bacterial Foraging Algorithm (BFA), Bee's Algorithm (BA), Particle Swarm Optimization (PSO), etc...) were studied [4]-[6]. Another category of PID controllers is the Nonlinear PID (NLPID) that can be improved the dynamic response of the conventional PID controller [11]. The NLPID controller has the advantage of adaptive, self-learning, online adjustment, and relatively lower requirements for stability and precision of controlled objects. Moreover, the structure of the NLPID controller is simple and reliable [12].

An efficient covid-19 optimization algorithm to find the optimal values of the PD/PID cascaded controller was presented in [13]. A practical design and control for a delta robot based on a low-cost microcontroller were illustrated in [14]. A collocation method based on sinc function and Bernoulli wavelet is proposed to find numerical solution of pantograph Volterra fuzzy integro-differential equation was demonstrated in [15].

This paper presents the design steps for an enhanced optimal NLPID based on a flower pollination optimization algorithm. In the first step, the initial values of NLPID

control parameters can be estimated by try and error and this takes a long time for the simulation. In the second step, the tuning optimization techniques used usually rely on the computation of an objective function representing the desired performance while satisfying the system constraints [16]. So, the Flower Pollination (FP) based on an effective objective function will be used to find the optimal values of controller parameters [17].

II. PANTOGRAPH MECHANISM MODEL

A. Direct Kinematics

The constrain of the five-link mechanisms as shown in Fig. 3 is given by

$$L_1 \bar{a}_1 + L_2 \bar{b}_1 - L_3 \bar{c}_1 - L_4 \bar{d}_1 - L_5 \bar{n}_1 = 0 \quad (1)$$

where L_i for $i=1, \dots, 5$ is the length of links, $(\bar{a}_1, \bar{b}_1, \bar{c}_1, \bar{d}_1, \bar{n}_1)$ are unit vectors [7]. The relation between the task space $(X=(x_e, y_e)^T)$ and joint space $(\theta=(\theta_1, \theta_2, \theta_3, \theta_4)^T)$ of the five-link mechanism system can be calculated, where x and y are the Cartesian coordinates of Joint e with respect to the plane (n_1, n_2) [16], as shown in Fig. 3.

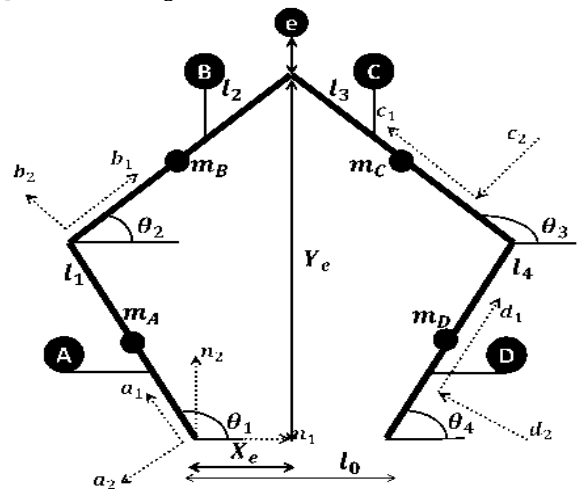


Figure 3. Direct kinematics mechanism.

The equations of x and y using θ_1 and θ_4 are defined as follows [17]:

$$x_e = L_1 \cos \theta_1 + L_2 \cos \theta_2 = L_3 \cos \theta_3 + L_4 \cos \theta_4 + L_5 \quad (2)$$

$$y_e = L_1 \sin \theta_1 + L_2 \sin \theta_2 = L_3 \sin \theta_3 + L_4 \sin \theta_4 \quad (3)$$

Equations (2) and (3) can simulate the forward kinematics of the five-link mechanism. From equations (1), (2), and (3) θ_2 can be expressed in terms of θ_1 and θ_4 by the holonomic constraints. Where θ_2 is dependent angle and has to be described using the active angle of the device (θ_1 and θ_4).

Newton-Raphson method or Trigonometry method can be used to find θ_3 and θ_2 . In this work, the trigonometry method was used as follows:

$$\theta_3 = 2 \tan^{-1} \left(\frac{A \pm \sqrt{A^2 + B^2 - C^2}}{B - C} \right) \quad (4)$$

where,

$$A = 2 L_3 L_4 \sin \theta_4 - 2 L_1 L_3 \cos \theta_1$$

$$B = 2L_3L_5-2L_1L_3 \cos \theta_1 +2L_4L_3 \cos \theta_4$$

$$C=L_1^2-L_2^2+L_3^2+L_4^2+L_5^2-L_1L_4 \sin \theta_1 \sin \theta_4 -2L_1L_5 \cos \theta_1 -2L_4L_5 \cos \theta_4 \cos \theta_1$$

And,

$$\theta_2 = \sin^{-1} \left(\frac{L_3 \sin \theta_3 + L_4 \sin \theta_4 - L_1 \sin \theta_1}{L_2} \right) \quad (5)$$

B. Inverse Kinematics

The direct relation between the coordinates of the end-effector and link lengths to the actuating angles θ_1 and θ_4 is in the following equations [18]:

$$\theta_1 = 2 \tan^{-1} \left(\frac{-E \pm \sqrt{D^2 + E^2 - F^2}}{-D - F} \right) \quad (6)$$

Where,

$$\begin{aligned} D &= x_e \\ E &= y_e \\ F &= \frac{L_1^2 - L_2^2 + x_e^2 + y_e^2}{2L_1} \end{aligned}$$

And

$$\theta_4 = 2 \tan^{-1} \left(\frac{-H \pm \sqrt{G^2 + H^2 - I^2}}{-G - I} \right) \quad (7)$$

Where,

$$\begin{aligned} G &= x_e - L_5 \\ H &= y_e \\ I &= \frac{L_4^2 + L_5^2 - L_3^2 - 2x_e L_5 + x_e^2 + y_e^2}{2L_4} \end{aligned}$$

The link lengths are constant for the robot, which helps to easily solve the above equations. From equations (12) and (17) it can be obtained θ_1 and θ_4 without known θ_2 and θ_3 [17]. The only inputs needed for controlling the five-link mechanism are the location of the end-effector (x_e and y_e).

C. Boundary Conditions

It is an important part which is the permissible boundary for a mechanism so that the link does not reach the singularity state during the path [19]. For this to be achieved Q_5 must not be equal to 180 degrees but rather greater.

So, $Q_5 < 180$ shown in Fig. 4

$$\begin{aligned} Q_5 &= 540 - (180 + \theta_1) - (180 - \theta_4 + \theta_3) \\ &\quad - (180 + \theta_1 - \theta_2) - (\theta_4) \end{aligned} \quad (8)$$

So the first boundary is:

$$Q_5 = (\theta_2 - \theta_3) < 180 \quad (9)$$

Second one: In order for the mechanism not to reach the position shown in Fig. 4, θ_2 must be greater than θ_1 .

Third one: θ_4 must be greater than θ_3 .

$$(\theta_2 > \theta_1) \quad (10)$$

$$(\theta_4 > \theta_3) \quad (11)$$

The three rules (9), (10), and (11), can be implemented using the logic gate (AND).

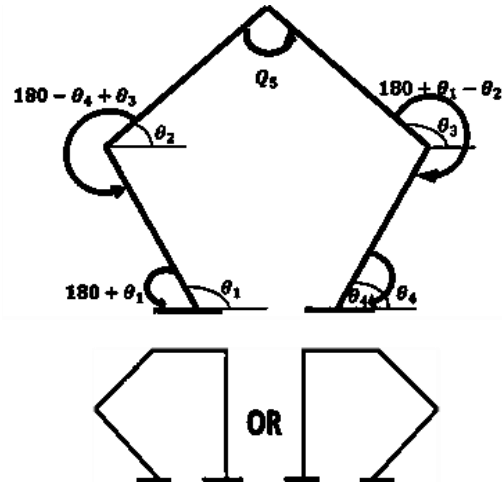


Figure 4. Direct kinematics mechanism.

D. Equation of Motion

Lagrangian equation:

$$T = \text{Torque} = \frac{\partial}{\partial t} \frac{\partial L}{\partial \dot{\theta}_i} - \frac{\partial L}{\partial \theta_i} \quad [18] \quad (12)$$

By using Lagrangian equation obtain by torque, T_1 and T_2 , Where (A, B, C, D, E, F) are constants.

$$\begin{aligned} T_1 &= (A_1 \ddot{\theta}_1 + B_1 \ddot{\theta}_4 + C_1 \dot{\theta}_1 + D_1 \dot{\theta}_4) \\ &\quad - (E_1 \dot{\theta}_1^2 + F_1 \dot{\theta}_4^2 + G_1 \dot{\theta}_1 \dot{\theta}_4) \end{aligned} \quad (13)$$

$$\begin{aligned} T_2 &= (A_2 \ddot{\theta}_1 + B_2 \ddot{\theta}_4 + C_2 \dot{\theta}_1 + D_2 \dot{\theta}_4) \\ &\quad - (E_2 \dot{\theta}_1^2 + F_2 \dot{\theta}_4^2 + G_2 \dot{\theta}_1 \dot{\theta}_4) \end{aligned} \quad (14)$$

where,

$$\begin{aligned} A_1 &= 2 (W_1 + W_4) + 2 (W_3 + W_5) Z_1^2 \\ &\quad + 2 W_6 Z_1 Z_5 + 2 Z_3^2 (W_7 + W_9) \end{aligned}$$

$$\begin{aligned} B_1 &= 2 Z_1 Z_2 (W_3 + W_5) + (W_6 + Z_2 + Z_5) \\ &\quad + 2 Z_3 Z_4 (W_7 + W_9) \\ &\quad + (W_{10} + Z_3 + Z_6 + Z_3 + Z_6) \end{aligned}$$

$$\begin{aligned} C_1 &= 4 (W_3 + W_5) Z_1 \frac{dZ_1}{dt} + 2 W_6 Z_1 \frac{dZ_5}{dt} \\ &\quad + 2 W_6 Z_5 \frac{dZ_1}{dt} + 4 (W_7 \\ &\quad + W_9) Z_3 \frac{dZ_3}{dt} \end{aligned}$$

$$D_1 = 2 (W_3 + W_5) Z_1 \frac{dZ_2}{dt} + 2 (W_3 + W_5) Z_2 \frac{dZ_1}{dt} + W_6 Z_2 \frac{dZ_5}{dt} + W_6 Z_5 \frac{dZ_2}{dt} + 2 (W_7 + W_9) Z_3 \frac{dZ_4}{dt} + W_{10} Z_6 \frac{dZ_3}{dt}$$

$$E_1 = 2 (W_3 + W_5) Z_1 \frac{dZ_1}{d\theta_1} + 2 (W_7 + W_9) Z_3 \frac{dZ_3}{d\theta_1} + W_6 Z_1 \frac{dZ_5}{d\theta_1} + W_6 Z_5 \frac{dZ_1}{d\theta_1}$$

$$F_1 = 2 (W_3 + W_5) Z_2 \frac{dZ_2}{d\theta_1} + 2 (W_7 + W_9) Z_4 \frac{dZ_4}{d\theta_1} + W_{10} Z_4 \frac{dZ_6}{d\theta_1} + W_{10} Z_6 \frac{dZ_4}{d\theta_1}$$

$$G_1 = 2 (W_3 + W_5) Z_1 \frac{dZ_2}{d\theta_1} + 2 (W_3 + W_5) Z_2 \frac{dZ_1}{d\theta_1} + W_6 Z_2 \frac{dZ_5}{d\theta_1} + W_6 Z_5 \frac{dZ_2}{d\theta_1} + 2 (W_7 + W_9) Z_3 \frac{dZ_4}{d\theta_1} + 2 (W_7 + W_9) Z_4 \frac{dZ_3}{d\theta_1} + W_9 Z_4 \frac{dZ_3}{d\theta_1} + W_{10} Z_3 \frac{dZ_6}{d\theta_1} + W_{10} Z_6 \frac{dZ_3}{d\theta_1}$$

$$A_2 = 2 (W_3 + W_5) Z_1 Z_2 + W_6 Z_2 Z_5 + 2 (W_7 + W_9) Z_3 Z_4 + W_{10} Z_3 Z_6$$

$$B_2 = 2 (W_2 + W_8) + 2 (W_3 + W_5) Z_2^2 + 2 (W_7 + W_9) Z_4^2 + (W_{10} + Z_4 + Z_6)$$

$$C_2 = 2 (W_3 + W_5) Z_1 \frac{dZ_2}{dt} + 2 (W_3 + W_5) Z_2 \frac{dZ_1}{dt} + W_6 Z_2 \frac{dZ_5}{dt} + W_6 Z_5 \frac{dZ_2}{dt} + 2 (W_7 + W_9) Z_3 \frac{dZ_4}{dt} + 2 (W_7 + W_9) Z_4 \frac{dZ_3}{dt} + W_{10} Z_3 \frac{dZ_6}{dt} + W_{10} Z_{10} \frac{dZ_3}{dt}$$

$$D_2 = 4 (W_3 + W_5) Z_2 \frac{dZ_2}{dt} + 4 (W_7 + W_9) Z_4 \frac{dZ_4}{dt} + 2 W_{10} Z_4 \frac{dZ_6}{dt} + 2 W_{10} Z_6 \frac{dZ_4}{dt}$$

$$E_2 = 2 (W_3 + W_5) Z_1 \frac{dZ_1}{d\theta_4} + W_6 Z_1 \frac{dZ_5}{d\theta_4} + W_6 Z_5 \frac{dZ_1}{d\theta_4} + 2 (W_7 + W_9) Z_3 \frac{dZ_3}{d\theta_4}$$

$$F_2 = 2 (W_3 + W_5) Z_2 \frac{dZ_2}{d\theta_4} + 2 (W_7 + W_9) Z_4 \frac{dZ_4}{d\theta_4} + W_{10} Z_4 \frac{dZ_6}{d\theta_4} + W_{10} Z_6 \frac{dZ_4}{d\theta_4}$$

$$G_2 = 2 (W_3 + W_5) Z_1 \frac{dZ_2}{d\theta_4} + 2 (W_3 + W_5) Z_2 \frac{dZ_1}{d\theta_4} + W_6 Z_2 \frac{dZ_5}{d\theta_4} + W_6 Z_5 \frac{dZ_2}{d\theta_4} + 2 (W_7 + W_9) Z_3 \frac{dZ_4}{d\theta_4} + W_{10} Z_6 \frac{dZ_3}{d\theta_4} + 2 (W_7 + W_9) Z_4 \frac{dZ_3}{d\theta_4} + W_{10} Z_3 \frac{dZ_6}{d\theta_4}$$

An explanation of the details of the variables mentioned in the previous equations is attached in the Appendix.

III. OPTIMAL NONLINEAR PID CONTROL

A. PID Control

It is well known that the transfer function of the linear PID controller is $K(s) = K_p + K_i/s + K_d s$. Where K_p , K_i and K_d are fixed gains. These gains can be defined as follows: K_p is the proportional gain which attempts to reduce the error responses, K_i is the integral gain and its role is to dampen the steady-state error, and K_d is the differential gain which decreases the overshoot of the system. Also, it ensures system stability [18], [19].

Despite linear fixed parameters PID controllers are often suitable for controlling a simple physical process, the demands for high-performance control with different operating point conditions or environmental parameters are often beyond the abilities of simple PID controllers [12], [20]. The performance of linear PID controllers can be enhanced using several techniques which will be developed to deal with sudden disturbances and complex systems, for example, the PID self-tuning methods, neural networks, fuzzy logic strategies, and other methods [21], [22].

Among these techniques, nonlinear PID (NLPID) control is presented as one of the most appropriate and effective methods for industrial applications. The nonlinear PID (NLPID) control is carried out in two broad categories of applications. The first category is particular to nonlinear systems, where NLPID control is used to absorb the nonlinearity. The second category deals with linear systems, where NLPID control is used to obtain enhanced performance not realizable by a linear PID control, such as reduced over-shoot, diminished rise time for the step or rapid command input, obtained better-

tracking accuracy and used to compensate the nonlinearity and disturbances in the system [23]. The NLPID controllers have the advantage of high initial gain to achieve a fast dynamic response, followed by a low gain to avoid unstable behavior. In this study, the traditional linear PID controller can be enhanced by combining a sector-bounded nonlinear gain into linear fixed gain PID control architecture.

B. Nonlinear PID Control

The proposed enhanced nonlinear PID (NLPID) controller consists of two parts. The first part is a sector-bounded nonlinear gain $K_n(e)$ while the second part is a linear fixed-gain PID controller (K_p, K_i and K_d). The nonlinear gain $K_n(e)$ is a sector-bounded function of the error $e(t)$. The previous research has been considered the nonlinear gain $K_n(e)$ as a one scalar value.

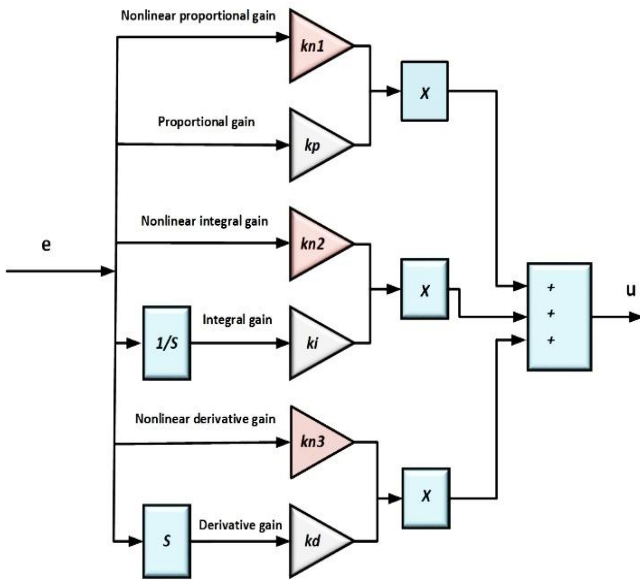


Figure 5. The enhanced nonlinear PID controller structure.

The new in this research, the one scalar value of $K_n(e)$ will be replaced with a row vector that can be expressed as $K_n(e) = [K_{n1}(e) \ K_{n2}(e) \ K_{n3}(e)]$ as shown in Fig. 5 which will lead to improving the performance of nonlinear PID controller where the values of nonlinear gains will be adjusted according to the error and the type of fixed parameters (K_p, K_i and K_d).

The proposed form of NLPID control can be described as follows.

$$u(t) = K_p [K_{n1}(e) \cdot e(t)] + K_i \int_0^t [K_{n2}(e) \cdot e(t)] dt + K_d \left[K_{n3}(e) \cdot \frac{de(t)}{dt} \right] \tag{15}$$

where $K_{n1}(e), K_{n2}(e)$ and $K_{n3}(e)$ are nonlinear gains. The nonlinear gains represent any general nonlinear function of the error which is bounded in the sector $0 < K_n(e) < K_n(e)_{max}$.

There is a wide range of choices available for the nonlinear gain $K_n(e)$. One simple form of the nonlinear gain function can be described as.

$$K_{ni}(e) = ch(w_i e) = \frac{\exp(w_i e) + \exp(-w_i e)}{2} \tag{16}$$

where $i = 1, 2, 3$.

$$e = \begin{cases} e & |e| \leq e_{max} \\ e_{max} \operatorname{sgn}(e) & |e| > e_{max} \end{cases} \tag{17}$$

The nonlinear gain $K_n(e)$ is lower bounded by $K_n(e)_{min} = 1$ when $e = 0$, and upper-bounded by $K_n(e)_{max} = ch(w_i e_{max})$. Therefore, e_{max} stand for the range of deviation, and w_i describes the rate of variation of $K_n(e)$.

The critical point in the PID and NLPID controllers is selecting the proper parameters to be appropriate for the controlled plant.

There are different approaches to finding the parameters of PID controller, for instance, try and error and Ziegler-Nichols method but, most of these approaches are rough roads. In this paper, the flower pollination optimization technique will be used to obtain the optimal values of both PID and NLPID controllers.

C. The Flower Pollination (FP)

In nature, the objective of flower pollination (FP) is the survival of the fittest and optimal reproduction of flowering plants. Pollination in flowering plants can take two major forms, i.e. biotic and abiotic [11]. About 90% of flowering plants belong to biotic pollination. Pollen is transferred by pollinators such as bees, birds, insects, and animals about 10% remaining of pollination take abiotic such as wind and diffusion in water. Pollination can be achieved by self-pollination or cross-pollination. Self-pollination is the fertilization of one flower from the pollen of the same flower (Autogamy) or different flowers of the same plant (Geitonogamy).

They occur when the flower contains both male and female gametes. Self-pollination usually occurs at a short distance without pollinators. It is regarded as local pollination. Cross-pollination, Allogamy, occurs when pollen grains are moved to a flower from another plant.

The process happens with the help of biotic or abiotic agents as pollinators. Biotic, cross-pollination may occur at a long distance with biotic pollinators. It is regarded as global pollination. Bees and birds as biotic pollinators behave Lévy flight behavior [24] with jump or fly distance steps obeying a Lévy distribution. The FPA algorithm was proposed by Yang [25].

The FP optimization has been used to determine the optimal values for the six parameters that are important in the design of the NLPID control, these parameters are K_p, K_i, K_d, w_1, w_2 and w_3 . The used objective function for this purpose is as follows equation (18).

$$f = \frac{1}{(1 - e^{-\beta})(M_p + e_{ss}) + e^{-\beta}(t_s - t_r)} \tag{18}$$

The actual closed-loop specification of the system with controller, rise time (t_r), maximum overshoot (M_p), settling time (t_s), and steady-state error (e_{ss}).

This objective function can fulfill the designer's requirement using the weighting factor value (β). The factor is set larger than 0.7 to reduce overshoot and steady-state error. If this factor is set smaller than 0.7 the rise time and settling time will be reduced [26].

Comparison between Nonlinear PID Controller and PID Controller by using flower pollination algorithm to optimize the performance of variables as shown in the Table below:

TABLE I. PARAMETERS VALUE

PID	NLPID
$K_p = 20$	$K_p = 90$
$K_i = 3$	$K_i = 3.5$
$K_d = 5$	$K_d = 1.3$
-	$W_1 = 0.19$
-	$W_2 = 3$
-	$W_3 = 1.14$

IV. SIMULATION RESULTS

The required path is a rectangle shown in Fig. 6 with the coordinates for the four corners as follows: home position (-0.1, 0.373), starter point (-0.05, 0.36), first corner (-0.05, 0.35), second corner (-0.14, 0.35), third corner (-0.14, 0.25), fourth corner (-0.05, 0.25).

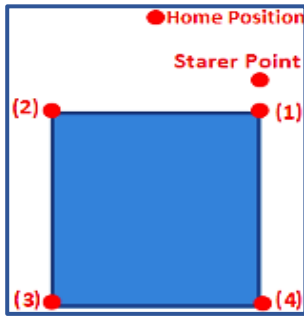
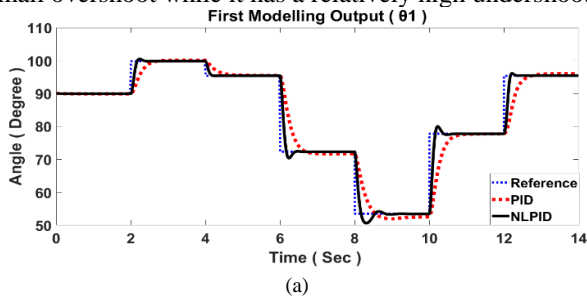


Figure 6. Required trajectory.

The dynamic response of θ_1 for each control technique applied to the pantograph model was shown in Fig. 7. It can be noted the FP-based NLPID controller has a faster response compared to the FP-based PID controller. Also, the FP-based PID controllers suffer from high steady-state error. It can be noted that the FP-based NLPID controller performance dynamic response is better than the recent research [27].

Moreover, the FP-based NLPID controller has a very small overshoot while it has a relatively high undershoot.



(a)

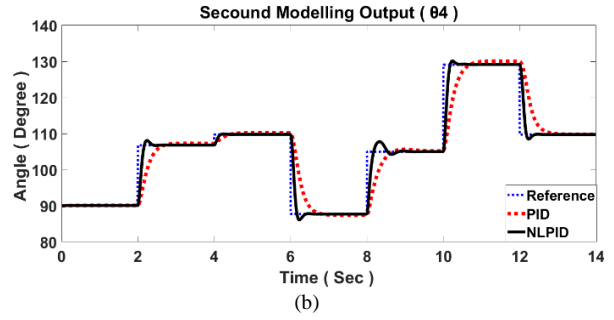


Figure 7. The position response of θ_1 and θ_4 through the control techniques.

The corresponding velocity responses of θ_1 and θ_4 for control techniques were demonstrated in Fig. 8. It is obvious that the FP-based NLPID controller has a high-velocity response compared to the FP-based PID controller. Also, the velocity peak of the FP-based PID controller is very low in contrast to the FP-based NLPID controller.

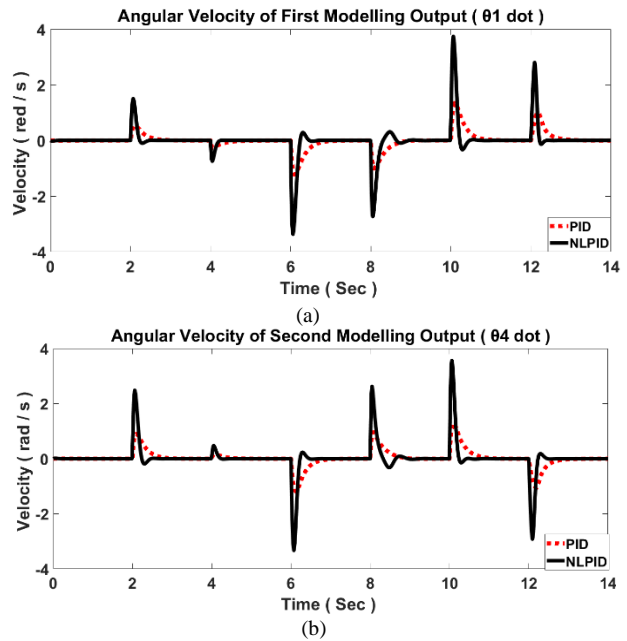
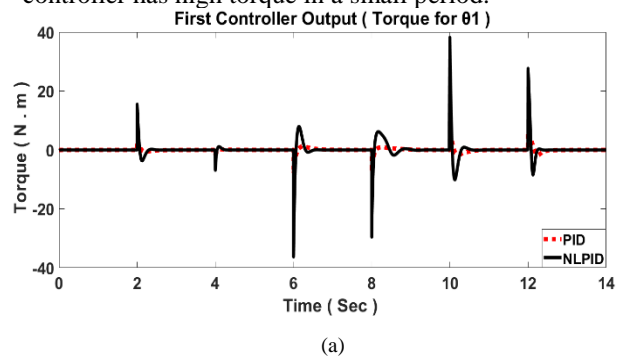


Figure 8. The velocity of both modeling output: velocity of θ_1 and θ_4 both as m/s.

Fig. 9 illustrates the corresponding output torque of controllers. It is clear that the FP-based NLPID controller generates a high torque compared to the FP-based PID controller. Also, the torque peak of the FP-based PID controller is very small while the FP-based NLPID controller has high torque in a small period.



(a)

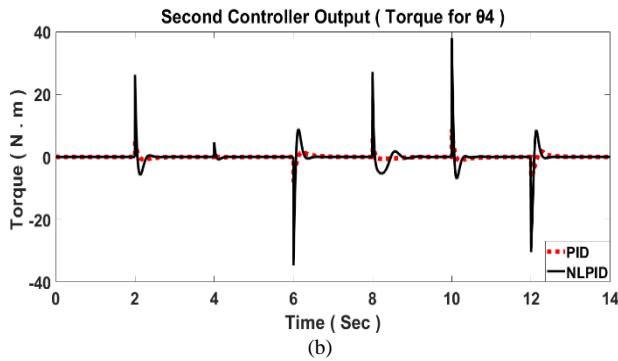


Figure 9. The controller output (torque) is shown for the first controller and the second one respectively.

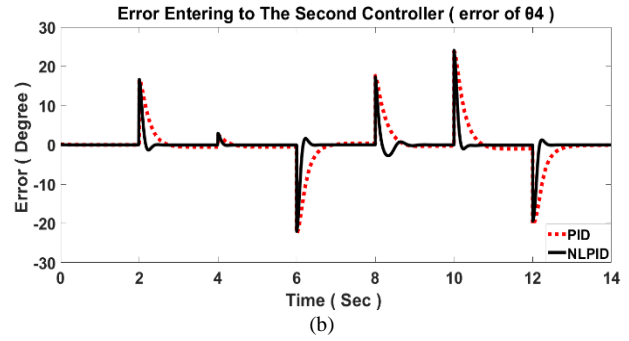


Figure 11. The entering error to the controller is shown for the first controller and the second one.

Fig. 10 displays the trajectory planning of controllers. It is clear that the FP-based NLPID controller has high accuracy compared to the FP-based PID controller. Also, it can be noted that high deviation for both controllers through the transition from horizontal line to vertical line due to the sharp corner.

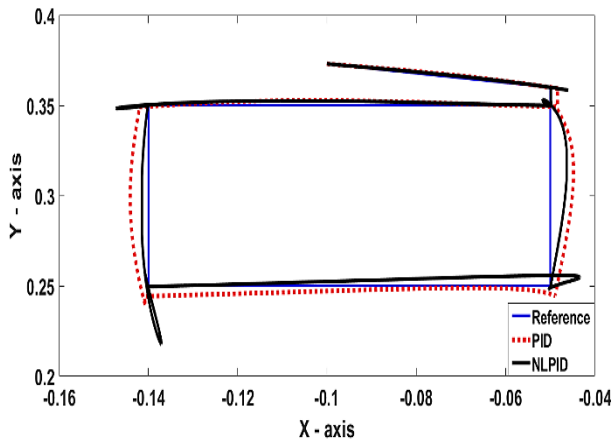


Figure 10. The controller output (torque) is shown for the first controller and the second one respectively.

The trajectory planning errors of each control technique was displayed in Fig. 11. It is obvious that the FP-based NLPID controller has low error compared to the FP-based PID controller. Also, the mean square error value of proposed control techniques has been demonstrated in Table I.

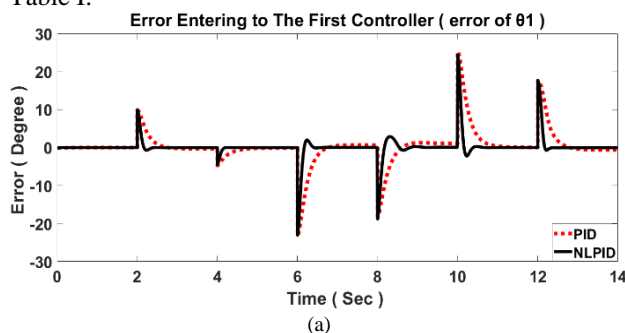


Table II demonstrates the performance of the pantograph by using the PID controller. It can be noted the error in the x-direction is 6.9% while the error in the y-direction is 0.15%. in contrast to the research [27], the trajectory with a maximum error of 17.2%. Then this model was tested using the PID control also, on a circuit-shaped trajectory with a maximum error of 11%

TABLE II. PID CONTROLLER COMPARED TO THE DESIRE

PID			
Reference Values		Real Values	
X	Y	X	Y
-0.08825	0.333675	-0.0825074	0.33417685
The Difference of X		The Difference of Y	
0.005742582		0.000501853	
The Error of X (%)		The Error of Y (%)	
6.960080251		0.150175798	

Table III displays the performance of the pantograph by using the NLPID controller. It is clear that the error percentage will be decreased compared to the PID controller. It is clear that the system performance was improved using the proposed FP-based NLPID controller compared to the recent research [27].

TABLE III. NLPID CONTROLLER COMPARED TO THE DESIRE

NLPID			
Reference Values		Real Values	
X	Y	X	Y
-0.08825	0.333675	-0.089533	0.3367585
The Difference of X		The Difference of Y	
-0.001283172		0.003083471	
The Error of X %		The Error of Y %	
1.43318043		0.915632853	

Table IV illustrates the performance of the pantograph by using NLPID controller compared to PID controller:

TABLE IV. NLPID CONTROLLER COMPARED TO PID CONTROLLER

The Difference of Value between PID & NLPID for X	0.007025754
The Difference of Value between PID & NLPID for Y	0.002581618
The Difference of Errors between PID & NLPID % for X	8.39326068
The Difference of Errors between PID & NLPID % for Y	0.765457056

V. CONCLUSION

This paper presents a new mathematical model for a closed chain pantograph mechanism, where the boundary conditions are considered. An overall MATLAB Simulink has been implemented to describe the dynamic behavior of the pantograph robot mechanism. The proposed mathematical model for the pantograph and the corresponding model mechanism using the Simscape were validated to give the same results. Moreover, two control techniques were designed. The first control presents the PID controller which had adjusted by Flower Pollination (FP) optimization. The second control is Nonlinear PID (NLPID) controller where its parameters were determined by Flower Pollination (FP) optimization based on a certain objective function. A rectangle trajectory position reference is applied to the end effector of the pantograph robot. This purpose was done by the proposed controllers to ensure robustness and performance. The simulation results offer that the FP-Based NLPID controller-based FP gives more accuracy and better performance compared to the PID controller. The end effector has a less rise time and settling time with high accuracy and low vibration at the FP- Based NLPID controller.

APPENDIX

$$\begin{aligned}
 W_1 &= \frac{1}{6} m_A L_1^2 & W_2 &= \frac{1}{6} m_D L_4^2 \\
 W_3 &= \frac{1}{24} m_B L_2^2 & W_4 &= \frac{1}{2} m_B L_1^2 \\
 W_5 &= \frac{1}{8} m_B L_2^2 & W_6 &= \frac{1}{2} m_B L_1 L_2 \\
 W_7 &= \frac{1}{24} m_C L_3^2 & W_8 &= \frac{1}{2} m_C L_4^2 \\
 W_9 &= \frac{1}{8} m_C L_3^2 & W_{10} &= \frac{1}{4} m_C L_3 L_4 \\
 Z_1 &= \frac{\partial \theta_2}{\partial \theta_1} = \frac{L_1 \sin(\theta_3 - \theta_1)}{L_2 \sin(\theta_2 - \theta_3)} & Z_2 &= \frac{\partial \theta_2}{\partial \theta_4} = \frac{L_4 \sin(\theta_4 - \theta_3)}{L_2 \sin(\theta_2 - \theta_3)}
 \end{aligned}$$

$$\begin{aligned}
 Z_3 &= \frac{\partial \theta_3}{\partial \theta_1} = \frac{L_1 \sin(\theta_2 - \theta_1)}{L_3 \sin(\theta_2 - \theta_3)} & Z_4 &= \frac{\partial \theta_3}{\partial \theta_4} = \frac{L_4 \sin(\theta_4 - \theta_2)}{L_3 \sin(\theta_2 - \theta_3)} \\
 Z_5 &= \cos(\theta_1 - \theta_2) & Z_6 &= \cos(\theta_3 - \theta_4)
 \end{aligned}$$

CONFLICT OF INTEREST

The authors declare no conflict of interest.

AUTHOR CONTRIBUTIONS

Layla M EL-Tehewy: Implementation the overall simulation and collect the results. Mohamed A. Shamseldin: Design and analysis the proposed control techniques. Mohamed Sallam: Build the system pantograph system model. A. M. Abdel Ghany: Analysis the results and manuscript revision.

ACKNOWLEDGMENT

The authors would like to offer thanks to Dr. Mohamed Abdel-Ghany, Faculty of Engineering, 6th October University, for his great efforts in this paper

REFERENCES

- [1] B. Zi, J. Cao, and Z. Zhu, "Dynamic simulation of hybrid-driven planar five-bar parallel mechanism based on simmechanics and tracking control," *Int. J. Adv. Robot. Syst.*, vol. 8, no. 4, pp. 28–33, 2011.
- [2] I. Chavdarov, "Kinematics and force analysis of a five-link mechanism by the four spaces Jacoby Matrix," *Probl. Eng. Cybern. Robot.*, pp. 53–63, 2005.
- [3] S. Jian and L. Rolland, "Imece2014-37602 five bar planar manipulator simulation and analysis by bond," in *Proc. ASME 2014 International Mechanical Engineering Congress and Exposition*, 2014, pp. 1–7.
- [4] R. Hosseinzadeh and M. Zarebnia, "Application and comparison of the two efficient algorithms to solve the pantograph volterra fuzzy integro-differential equation," *Soft Comput.*, vol. 25, no. 10, pp. 6851–6863, 2021.
- [5] S. Kosari, Z. Shao, M. Yadollahzadeh, and Y. Rao, "Existence and uniqueness of solution for quantum fractional pantograph equations," *Iran. J. Sci. Technol. Trans. A Sci.*, vol. 1, 2021.
- [6] J. W. Yoon, J. Ryu, and Y. K. Hwang, "Optimum design of 6-DOF parallel manipulator with translational/rotational workspaces for haptic device application," *J. Mech. Sci. Technol.*, vol. 24, no. 5, pp. 1151–1162, 2010.
- [7] C. M. Pappalardo, M. C. De Simone, and D. Guida, "Multibody modeling and nonlinear control of the pantograph/catenary system," *Arch. Appl. Mech.*, vol. 89, no. 8, pp. 1589–1626, 2019.
- [8] G. Campion, Q. Wang, and V. Hayward, "The pantograph Mk-II: A haptic instrument," in *Proc. IEEE/RSJ Int. Conf. Intell. Robot. Syst. IROS*, pp. 723–728, 2005.
- [9] J. Pilecki, M. A. Bednarczyk, and W. Jamroga, "Model checking properties of multi-agent systems with imperfect information and imperfect recall," in *Intelligent Systems*, 2014.
- [10] M. A. Rushdi, A. A. Hussein, T. N. Dief, S. Yoshida, and R. Schmehl, "Simulation of the transition phase for an optimally-controlled tethered vtol rigid aircraft for airborne wind energy generation," *AIAA Scitech 2020 Forum*, no. 1, pp. 1–12, 2020.
- [11] R. S. U. Raju, V. V. S. S. Chakravarthy, and P. S. R. Chowdary, "Flower pollination algorithm based reverse mapping methodology to ascertain operating parameters for desired surface roughness," *Evol. Intell.*, vol. 14, no. 2, pp. 1145–1150, 2021.

- [12] Y. X. Su, D. Sun, and B. Y. Duan, "Design of an enhanced nonlinear PID controller," *Mechatronics*, vol. 15, pp. 1005–1024, 2005.
- [13] M. A. Shamseldin, "Optimal Covid-19 based PD/PID cascaded tracking control for robot arm driven by BLDC motor," *Wseas Trans. Syst.*, vol. 20, pp. 217–227, 2021.
- [14] E. Emad, O. Alaa, M. Hossam, M. Ashraf, and M. A. Shamseldin, "Design and implementation of a low-cost microcontroller-based an industrial delta robot," *Wseas Trans. Comput.*, vol. 20, pp. 289–300, 2021.
- [15] R. Hosseinzadeh and M. Zarebnia, "Application and comparison of the two efficient algorithms to solve the pantograph Volterra fuzzy integro-differential equation," *Soft Comput.*, vol. 25, no. 10, pp. 6851–6863, 2021.
- [16] Z. Sabir, M. A. Z. Raja, D.-N. Le, and A. A. Aly, "A neuro-swarming intelligent heuristic for second-order nonlinear Lane-Emden multi-pantograph delay differential system," *Complex Intell. Syst.*, no. 0123456789, 2021.
- [17] S. Lukasik, "Study of flower pollination algorithm for continuous optimization," *Adv. Intell. Syst. Comput.*, vol. 322, pp. 451–459, 2014.
- [18] L. Abdullah, *et al.*, "Evaluation on tracking performance of PID, gain scheduling and classical cascade P / PI controller on XY table ballscrew drive system faculty of manufacturing engineering, Universiti Teknikal Malaysia Melaka (UteM)," *World Appl. Sci. J. 21(Special Issue Eng. Technol.)*, vol. 21, pp. 1–10, 2013.
- [19] T. Nadu and P. Magnet, "Modeling and implementation of intelligent commutation system for BLDC motor in underwater robotic applications," in *Proc. 1st IEEE International Conference on Power Electronics. Intelligent Control and Energy Systems, Modeling*, 2016, pp. 1–4.
- [20] S. B. U, "Multivariable centralized fractional order PID controller tuned using harmony search algorithm for two interacting conical tank process," in *Proc. SAI Intelligent Systems Conference*, London, UK Multivariable, 2015, pp. 320–327.
- [21] P. Zhao and Y. Shi, "Robust control of the A-axis with friction variation and parameters uncertainty in five-axis CNC machine tools," *J. Mech. Eng. Sci.*, 2014.
- [22] B. B. Reddy, "Modelling and control of 2-DOF robotic manipulator using BLDC motor," *Int. J. Sci. Eng. Technol. Res.*, vol. 3, no. 10, pp. 2760–2763, 2014.
- [23] M. A. A. Ghany, M. A. Shamseldin, and A. M. A. Ghany, "A novel fuzzy self tuning technique of single neuron PID controller for brushless DC motor," *Int. J. Power Electron. Drive Syst.*, vol. 8, no. 4, pp. 1705–1713, 2017.
- [24] A. A. A. El-Samahy and A. A. A. El-Gammal, "Adaptive tuning of a PID speed controller for DC motor drives using multi-objective particle swarm optimization MOPSO," in *Proc. 11th International Conference on Computer Modelling and Simulation*, 2009.
- [25] N. A. Elkhateeb and R. I. Badr, "Novel PID tracking controller for 2DOF robotic manipulator system based on artificial bee colony algorithm," *Electr. Control Commun. Eng.*, vol. 13, no. 1, pp. 55–62, 2017.
- [26] M. A. Shamseldin, M. Sallam, A. M. Bassiuny, and A. M. A. Ghany, "A new model reference self-tuning fractional order PD control for one stage servomechanism system," *WSEAS Trans. Syst. Control*, vol. 14, pp. 8–18, 2019.
- [27] Z. Saeed, B. Gabra, M. Sallam, W. Refeay, and S. Sharaf, "Modeling and control of a pantograph mechanism interacting with the environment," in *Proc. International Conference on Advanced Machine Learning Technologies and Applications*, 2021.



Researcher Layla El-Tehewy obtained a Bachelor's degree in mechatronics engineering from the faculty of engineering, Modern Technology and Information University (MTI), Cairo, Egypt, accredited by the University of Wales in the UK in 2015. Once the academic graduation certificate was awarded Layla was appointed a faculty member at MTI University. In 2016, a master's degree was registered. In 2020, the master's thesis has been registered, and the degree is expected to be obtained during this year (2022).



Dr. Shamseldin obtained the Bachelor of mechatronics engineering in 2010 from faculty of engineering, Helwan University, Cairo, Egypt. In 2016, he obtained an M.Sc. in system automation from faculty of engineering, Helwan University, Cairo, Egypt. In 2020, he obtained a Ph.D. in Mechatronics Engineering from faculty of engineering, Helwan University, Cairo, Egypt. Also, Mohamed was a member of mobility staff to teach in a summer course at the University of Central Lancashire, Preston, UK. .



Mohamed Sallam was born in Egypt. He is lecturer at the department of mechanical engineering, faculty of engineering, Helwan University, His research interests include fuzzy control, neuro-fuzzy, and adaptive control system theories and their applications. He involved in two main research activities; first, magnetic teleoperation control of micro-particles where an image based control is used to control the position of a micro-particle floating in the water. The micro-particle has no actuators on-board. Instead, four perpendicular coils can generate the required magnetic field to move the particle in the x-y plane. The reference signal is sent using a haptic device that consists of a pantograph mechanism with two motors and two encoders. The research goal is to develop and compare different control schemes to have position tracking. On the other side, I am working with some industrial organizations to develop mechatronic products that can solve real problems in the country.



A.M. Abdel Ghany was born in Cairo. He received his B.Sc. and M.Sc. degrees in 1980 and 1987 from the Electrical Power System and Machines department, Helwan University , Cairo, Egypt. From 1989 to 1994, he got his Ph.D. in Computer Controlled Systems from the Institute of Control and Systems Engineering, Technical University of Wroclaw Poland. From 1994 to 1999, he worked as an assistant professor at the department of Electrical Machines and Power System, Helwan University, Cairo Egypt. In 2002, he was promoted to Associate Professor at the Department of Electrical Power Systems and Machines Department, University of Helwan, Cairo, Egypt. Currently, he was a lecturer at the Electrical Technology department, College of Technology at Al-Baha, Al-Baha, KSA. Dr. Abdel Ghany shared in the Economical Lighting of Helwan industrial plant as a part of the Supreme Council of Egyptian Universities Projects. He authored more than 114 papers in control and analysis of Power Systems.

Copyright © 2022 by the authors. This is an open access article distributed under the Creative Commons Attribution License ([CC BY-NC-ND 4.0](https://creativecommons.org/licenses/by-nc-nd/4.0/)), which permits use, distribution and reproduction in any medium, provided that the article is properly cited, the use is non-commercial and no modifications or adaptations are made.